ISSN 1674-1056
http://cpb.iphy.ac.cn
http://iopscience.iop.org/cpb
中国物理 B
Chinese Physics
中国物理
Chinese Physics B

Hybrid linear amplifier-involved detection for continuous variable quantum key distribution with thermal states

Yu-Qian He(贺宇千), Yun Mao(毛云), Hai Zhong(钟海), Duang Huang(黄端), Ying Guo(郭迎)
Citation: Chin. Phys. B . 2020, 29(5): 050309 . **doi:** 10.1088/1674-1056/ab8216
Journal homepage: http://cpb.iphy.ac.cn; http://iopscience.iop.org/cpb

What follows is a list of articles you may be interested in

Reconciliation for CV-QKD using globally-coupled LDPC codes

Jin-Jing Shi(石金晶), Bo-Peng Li(李伯鹏), Duan Huang(黄端)
Chin. Phys. B . 2020, 29(4): 040301 . **doi:** 10.1088/1674-1056/ab6d4f

Temperature effects on atmospheric continuous-variable quantum key distribution

Shu-Jing Zhang(张淑静), Hong-Xin Ma(马鸿鑫), Xiang Wang(汪翔), Chun Zhou(周淳), Wan-Su Bao(鲍皖苏), Hai-Long Zhang(张海龙)
Chin. Phys. B . 2019, 28(8): 080304 . **doi:** 10.1088/1674-1056/28/8/080304

Finite-size analysis of continuous-variable quantum key distribution with entanglement in the middle

Ying Guo(郭迎), Yu Su(苏玉), Jian Zhou(周健), Ling Zhang(张玲), Duan Huang(黄端)
Chin. Phys. B . 2019, 28(1): 010305 . **doi:** 10.1088/1674-1056/28/1/010305

Finite-size analysis of eight-state continuous-variable quantum key distribution with the linear optics cloning machine

Hang Zhang(张航), Yu Mao(毛宇), Duan Huang(黄端), Ying Guo(郭迎), Xiaodong Wu(吴晓东), Ling Zhang(张玲)
Chin. Phys. B . 2018, 27(9): 090307 . **doi:** 10.1088/1674-1056/27/9/090307

Continuous-variable quantum key distribution based on continuous random basis choice

Weiqi Liu(刘维琪), Jinye Peng(彭进业), Peng Huang(黄鹏), Shiyu Wang(汪诗寓), Tao Wang(王涛), Guihua Zeng(曾贵华)
Chin. Phys. B . 2018, 27(7): 070305 . **doi:** 10.1088/1674-1056/27/7/070305

Hybrid linear amplifier-involved detection for continuous variable quantum key distribution with thermal states*

Yu-Qian He(贺宇千)[1], Yun Mao(毛云)[1,†], Hai Zhong(钟海)[1], Duang Huang(黄端)[2], and Ying Guo(郭迎)[1]

[1] *School of Automation, Central South University, Changsha* 410083, *China*

[2] *School of Computer Science and Engineering, Central South University, Changsha* 410083, *China*

(Received 8 February 2020; revised manuscript received 7 March 2020; accepted manuscript online 23 March 2020)

Continuous-variable quantum key distribution (CVQKD) can be integrated with thermal states for short-distance wireless quantum communications. However, its performance is usually restricted with the practical thermal noise. We propose a method to improve the security threshold of thermal-state (TS) CVQKD by employing a heralded hybrid linear amplifier (HLA) at the receiver. We find the effect of thermal noise on the HLA-involved scheme in near-and-mid infrared band or terahertz band for direct and reverse reconciliation. Numerical simulations show that the HLA-involved scheme can compensate for the detriment of thermal noise and hence increase the security threshold of TS-CVQKD. In near-and-mid infrared band, security threshold can be extended by 2.1 dB in channel loss for direct reconciliation and 1.6 dB for reverse reconciliation, whereas in terahertz band, security threshold can be slightly enhanced for the gain parameter less than 1 due to the rise in thermal noise.

Keywords: continuous-variable quantum key distribution, thermal state, hybrid linear amplifier

PACS: 03.67.–a, 03.67.Dd, 03.67.Hk **DOI:** 10.1088/1674-1056/ab8216

1. Introduction

Continuous-variable quantum key distribution (CVQKD) allows two distant parties, Alice and Bob, to share random secret keys over an untrusted environment controlled by an eavesdropper, Eve.[1–4] Compared with discrete-variable quantum key distribution (DVQKD),[5–9] CVQKD can be applied on off-the-shelf optical fiber system with relative higher secret key rate, avoiding the imperfection for using single photon counting.[10,11] In a typical optical fiber system,[12–14] Alice encodes Gaussian-distributed random numbers on weak coherent states and then sends them to Bob through an optical fiber. However, such infrastructure is built on high power laser, may well be impractical for a plethora of attractive low-power ultra-high-speed quantum communications, such as WiFi, Bluetooth and chip-to-chip communications.[15] For example, customers in a supermarket may use mobile phone to scan the two-dimensional code wirelessly, in order to exchange secret keys with cash registers.

Unlike an optical fiber system that usually works in near infrared band,[16] modern wireless communication works in microwave and far infrared band.[17,18] In the above-mentioned frequency band, Alice may send thermal states to Bob instead of traditional coherent states because environment thermal noise is extremely high. Therefore, it is inevitable to deploy thermal-state CVQKD (TS-CVQKD) if we want to extend the application of quantum communication to a common wireless system. On the other hand, as the transmission rate of CVQKD has been growing dramatically over the years,[19,20] preparing quantum state precisely becomes challenging. Using TS-CVQKD will loosen the stringent requirements for optical amplitude and phase modulators since it needs no exact Guassian modulation.[21] Although TS-CVQKD is suitable to wireless communication and low cost to implement, thermal noise would dramatically reduce the actual performance of TS-CVQKD.[22,23] Thus, how to improve the performance of TS-CVQKD is a significance issue.

Currently, an amplifier has been used for combating the channel loss and other decoherence, resulting in the performance improvement of CVQKD.[24–28] The noiseless linear amplifier (NLA) is the most typical one.[24,29,30] It can increase the performance in a nondeterministic manner theoretically.[31,32] However, the actual success rate of a physical realization is far below the theoretical prediction owing to experimental limitation.[33] Alternative to the physical counterpart, the measurement-based noiseless linear amplifier (MB-NLA) is a virtualization version of NLA by simple data processing.[25] The MB-NLA offers a fully tunable cutoffs between probability and fidelity and hence more flexible. At the same time, a deterministic linear amplifier (DLA) can compensate for the imperfection of detector at receiver's side, leading to an improvement of maximal transmission distance.[26] However, the DLA cannot increase the signal-to-noise ratio (SNR) owing to the bosonic nature of photons.[34] Interestingly, a combination of DLA and MB-NLA, called the hybrid linear amplifier (HLA), was proposed and realized in experiments.[27] It inherits advantages of both MB-NLA and DLA and hence sets effective gain g_e free from success rate, which means one could fix g_e when the probability changes. It can be used to enhance the secret key rate and the transmission

*Project supported by the National Natural Science Foundation of China (Grant Nos. 61572529 and 61871407).

†Corresponding author. E-mail: maocsu@sina.com

© 2020 Chinese Physical Society and IOP Publishing Ltd

distance of the traditional CVQKD system.[35]

In this paper, we consider the deploy of HLA on Bob's side for the performance improvement of TS-CVQKD in near-and-mid infrared band or terahertz band. We find that in near-and-mid infrared band, the HLA-involved scheme can bring performance improvement of TS-CVQKD in direct reconciliation (DR), although the performance of the HLA-involved TS-CVQKD in reverse reconciliation (RR) is vulnerable to thermal noise. As the thermal radiation increases, the improved channel loss will decrease rapidly. In terahertz band, we find that DR is vastly superior to RR, where g_{DLA} plays a more important role than g_{NLA}. In addition, we find that the optimized g_{NLA} will lie in the area $g_{\mathrm{NLA}} < 1$ if we want to extend security threshold.

The rest of this paper is organized as follows. In Section 2, we propose the HLA-involved scheme for performance improvement of the TS-CVQKD system and demonstrate the interaction of g_{DLA} and g_{NLA}. In Section 3, we derive the secret key rate and security threshold in near-and-mid infrared band and terahertz band. Meanwhile, we achieve the suitable parameters g_{DLA} and g_{NLA} for maximizing security threshold of channel loss. Finally, we conclude in Section 4.

2. The HLA-involved TS-CVQKD

2.1. The scheme design of TS-CVQKD

The prepare and measure (PM) scheme of TS-CVQKD is shown in Fig. 1. Alice displaces thermal states with a bi-dimensional Gaussian distribution and sends signal model B_0 to Bob. The signal mode B_0 can be given by

$$\hat{x} = x_{\mathrm{m}} + \hat{x}_{\mathrm{s}}, \tag{1}$$

where x_{m} without a hat is the classical variable for the coded information and $\hat{x}_{\mathrm{s}}$ with a hat is an operator that denotes uncertain quantum noise. The vectorial operator $\hat{x}$ involves both quadratures $\hat{Q}$ and $\hat{P}$. The entire variance of signal state can be given by

$$V = V_{\mathrm{M}} + V_{\mathrm{S}}, \tag{2}$$

where V_{M} is modulated variance obeying Gaussian distribution and V_{S} is the shot noise variance, as shown in Fig. 1(c).

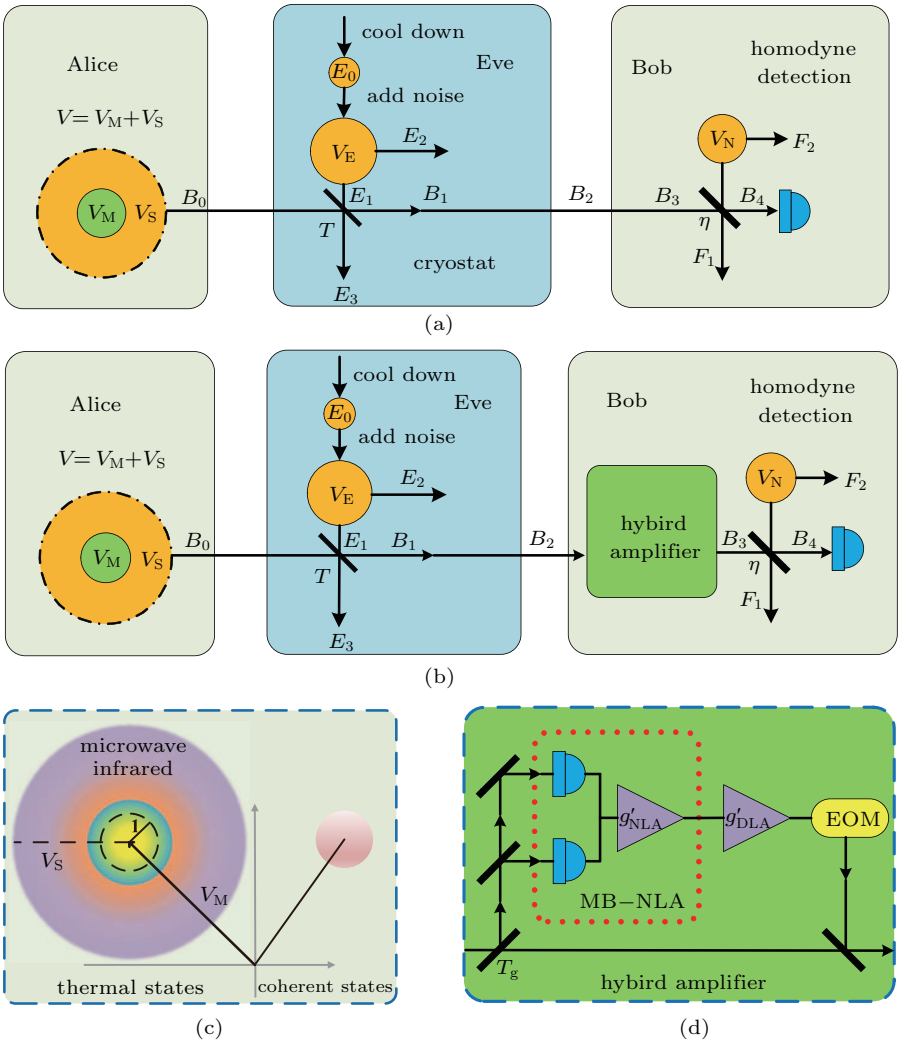


Fig. 1. (a) Schematic diagram of the standrad TS-CVQKD. (b)Schematic diagram of the HLA-involved TS-CVQKD. (c) Phase space representation of thermal state. As the frequency goes down from infrared regime to microwave regime, thermal noise would be enhanced. (d) Schematic of HLA achieved with a feed-forward loop. EOM, electro-optic modulator.

We assume that V_S is equal to 1 for unit vacuum shot-noise (SNU), as the yellow circular region shown in Fig. 1(c). As frequency band moves down from near infrared regime to microwave regime, however, the shot noise V_S will rise up and adapt to the environment noise. The environment noise over different frequencies is given by

$$V_S = N_0 = 2\bar{n} + 1, \tag{3}$$

where $\bar{n}$ is the average photon number for any wavelength given by[16]

$$\bar{n} = \frac{1}{\exp(hf/k_B T_K) - 1}, \tag{4}$$

where h is Planck's constant, f is the frequency of quantum signals, k_B is Boltzmann's constant, and T_K is the temperature. Even if without environment thermal fluctuations, thermal noise will still exist due to the imperfect modulation. Consequently, the shot noise V_S becomes $V_S = 1 + \mu$, where $\mu > 0$ is for the thermal state case and $\mu = 0$ is for the coherent state case.

Subsequently, signal mode B_0 goes through a noisy and lossy channel controlled by Eve, as depicted in Fig. 1. With the existing environment thermal noise, Eve has to first cool down her thermal mode E_0 so as to produce pure vacuum mode and then add known noise to the pure vacuum mode by modulating E_0. This added known noise should match the level of environment noise N_0 in order to cover her tracks.[16] Then, Eve performs an entangling cloner attack[36–38] by a beam splitter with transmission T and interacts one of her ancilla modes E_1 with B_0, resulting in B_1. E_3 and E_2 are stored in a quantum memory.

Finally, Bob performs homodyne detection to recover information. We model Bob's detection efficiency by a beam splitter with transmission efficiency η and detector electronics with v_{el}.[39] After collecting correlated strings from Alice, the postprocessing begins, which can be either DR or RR. For DR, the previous experiment result shows that TS-CVQKD is robust against thermal noise.[16] However, a channel loss of no more than 1.5 dB is possible,[23] which is not far enough for metropolitan transport networks. For RR, the performance would become terrible since the possible channel loss will rapidly decline to zero as thermal noise rises up.[23]

2.2. The HLA-involved scheme for enhancing TS-CVQKD

In what follows, we propose an approach for improving TS-CVQKD by inserting an HLA before Bob's detector, as shown in Fig. 1(b). Figure1(d) shows the practical implementation of HLA. When the signal mode enters the HLA, it will first pass through a beam splitter with transmission constant T_g given by[27]

$$T_g = g_{NLA}^2 / g_{DLA}^2. \tag{5}$$

The reflected mode is measured and selected via the MB-NLA, which virtualizes the physical NLA by Gaussian post-selection. It consists of a filter function and a rescaling factor whose probabilistic gain is g'_{NLA}.[40] The effect of the MB-NLA can be described as a covariance matrix (CM) transformation given by[31]

$$\begin{aligned} \gamma_{out} &= g_{NLA}[g_{NLA}^2 + 1 - \gamma_{in}(g_{NLA}^2 - 1)]^{-1} \\ &\quad \times [\gamma_{in}(g_{NLA}^2 + 1) - (g_{NLA}^2 - 1)]g_{NLA}^{-1}, \end{aligned} \tag{6}$$

$$d_{out} = 2g_{NLA}[g_{NLA}^2 + 1 - \gamma_{in}(g_{NLA}^2 - 1)]^{-1} d_{in}, \tag{7}$$

where γ_{in} and γ_{out} are covariance matrices of input and output respectively, and $g_{NLA} = \mathrm{Diag}(g_{NLA}, g_{NLA})$ is the amplifying matrix for the individual mode. For $g_{NLA} > 1$, the success probability can be given by[25]

$$P_{NLA} = \begin{cases} \exp(|x_m|^2 - |x_c|^2)(1 - g_{NLA}^{\prime -2}), & |x_m| \le x_c, \\ 1, & |x_m| \ge x_c, \end{cases} \tag{8}$$

where $x_m = (p_m + iq_m)/\sqrt{2}$ is the measurement outcome and x_c is the cutoff parameter which truncates the original post-selection filter in an appropriate amplitude and hence makes a trade-off between probability and fidelity. For $g_{NLA} < 1$, the success probability is given by

$$P_{NLA} = \frac{g_{NLA}^2}{g_{NLA}^2 + 2V_{in}(1 - g_{NLA}^2)}, \tag{9}$$

where V_{in} is the variance of input mode. After signal mode goes through the MB-NLA, it is further amplified by $g'_{DLA} = \sqrt{2(g_{DLA}^2 - 1)}$ times deterministically. Finally, the signal mode will be injected into the electro-optic modulator (EOM) to fulfill the displacement operation. The CM of output mode B_3 is given by

$$\gamma_{B_3} = \begin{pmatrix} \dfrac{g_{DLA}^2(V_{B_1} + 1) + g_{NLA}^2(V_{B_1} - 1)}{V_{B_1} + 1 - g_{NLA}^2(V_{B_1} - 1)} & 0 \\ 0 & \dfrac{g_{DLA}^2(V_{B_1} + 1) + g_{NLA}^2(V_{B_1} - 1)}{V_{B_1} + 1 - g_{NLA}^2(V_{B_1} - 1)} \end{pmatrix} \tag{10}$$

with $V_{B_1} = TV + (1 - T)V_E$. By solving for the singularity for the output Eq. (10), we can obtain the restriction of g_{NLA} given by

$$g_{NLA}^2 < (V_{B_1} + 1)/(V_{B_1} - 1). \tag{11}$$

In order to show how the HLA improves the performance of TS-CVQKD protocol, we compares the signal-to-noise ratio (SNR) of mode B_4 with and without HLA as shown in Fig. 1(b). When a thermal state passes through the HLA, the improvement of SNR at B_4 can be expressed as

$$\Delta\mathrm{SNR} = \mathrm{SNR}_{\mathrm{B_4with}} - \mathrm{SNR}_{\mathrm{B_4without}}. \tag{12}$$

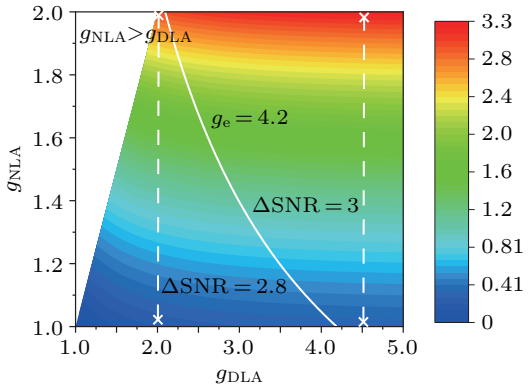


Fig. 2. The ΔSNR as functions of g_{NLA} and g_{DLA}. The blank area indicates unphysical region of $g_{\mathrm{NLA}} > g_{\mathrm{DLA}}$. The two white dashed lines represent ΔSNR when g_{NLA} changes from 1 to 2. The white solid line represents contour line of $g_e = g_{\mathrm{NLA}} g_{\mathrm{DLA}}$. Modulation variance $V_{\mathrm{M}} = 1$, shot noise $V_{\mathrm{S}} = 1.2$, transmission efficiency $\eta = 0.6$ and detector electronics $v_{\mathrm{el}} = 0.05$.

Figure 2 illustrates ΔSNR for the given parameters $V_{\mathrm{M}} = 1$, $V_{\mathrm{S}} = 1.2$, $v_{\mathrm{el}} = 0.05$ and $\eta = 0.6$. We find the larger the g_{NLA} or g_{DLA} means the more improvement of the SNR. In addition, the parameters g_{NLA} and g_{DLA} may have interacted with each other. For example, for $g_{\mathrm{DLA}} = 2$, a unit increase of g_{NLA} will give birth to the improved SNR by ΔSNR=2.8. For $g_{\mathrm{DLA}} = 4.5$, ΔSNR becomes 3. That is to say, g_{NLA} (g_{DLA}) may exhibit different effect when the other gain factor changes. Furthermore, we should point out the same effective gain $g_e = g_{\mathrm{NLA}} g_{\mathrm{DLA}}$ does not signify the same improvement of SNR.

Actually, we note the SNR improvement does not mean the increased secret key rates because it ignores the influence of Eve. The most typical example is the so-called fighting noise with noise,[41] where noise is added to the reference side to increase secret key rates when Eve's attack is strong. However, it may enhance the performance of TS-CVQKD for the tunable parameters in suitable ranges.

3. Security analysis

We demonstrate the performance improvement of the HLA-involved TS-CVQKD with the numerical simulations in near-and-mid infrared band (6 THz–400 THz) or terahertz band (60 GHz–1 THz). The secret key rates of TS-CVQKD with and without HLA are derived in Appendix B. Table 1 shows the parameters setting. In near-and-mid infrared band, the average photon number is very low and hence thermal noise is small, whereas thermal noise in terahertz band is extremely high. Consequently, the HLA-involved scheme makes a difference in terms of the secret key rates. In addition, the emerging terahertz band is identified as one of the promising spectrum bands to enable ultra-high-speed quantum communications.

Table 1. Parameter setting. The N–M represents near-and-mid infrared and T represents terahertz.

Symbol	Parameter setting	Value in N–M band	Value in T band
g_{NLA}	Gain of NLA	Independent variable	Independent variable
g_{DLA}	Gain of DLA	Independent variable	Independent variable
V_{S}	Shot noise	Independent variable	Independent variable
T	Transmission efficiency	Independent variable	Independent variable
f	Frequency	Independent variable	Independent variable
V_{E}	Channel noise	–	Independent variable
ε	Channel excess noise	0.05	–
V_{M}	Modulation variance	4	40
v_{el}	Electronic noise	0.05	0.05
η	Detection efficiency	0.6	0.6
β	Reconciliation efficiency	0.98[42]	0.98
T_{K}	Temperature	288	288

3.1. Near-and-mid infrared band

In near-and-mid infrared band, the performance of the HLA-involved TS-CVQKD is compared with standard TS-CVQKD in numerical simulations. We take into account the configuration of homodyne detection in both the DR and RR cases. As shown in Fig. 3, the thermal noise in near infrared band comes from imperfect modulation. Once the frequency exceeds a certain threshold in mid infrared regime, thermal noise will rise up quickly.

We find that the HLA can improve standard TS-CVQKD for both DR and RR in terms of security threshold as shown in Fig. 4. For DR, the added security threshold maintains at 1.8 dB as V_{S} changes, corresponding to an improvement over 125%. For RR, the added security threshold will decrease from 1.3 dB to 0.2 dB as V_{S} changes, leading to an improvement of no more than 6%. Then, we compare the performance of HLA-involved TS-CVQKD (dashed line) and LOCM-involved TS-CVQKD (dash-dotted line) in homodyne

detection. It is shown that inserting an HLA on Bob's side is better than inserting an LOCM no matter in DR or RR. For DR, LOCM even decreases the security threshold as compared to the standard protocol.

The performance of the HLA-involved TS-CVQKD will also be influenced by frequency f in DR. In Fig. 5, it shows that the security threshold can be extended by 2.1 dB for $f = 120$ THz, resulting in an improvement of 117% compared with the standard TS-CVQKD. However, when the frequency moves down to 6 THz, as shown in Fig. 5(b), the maximum

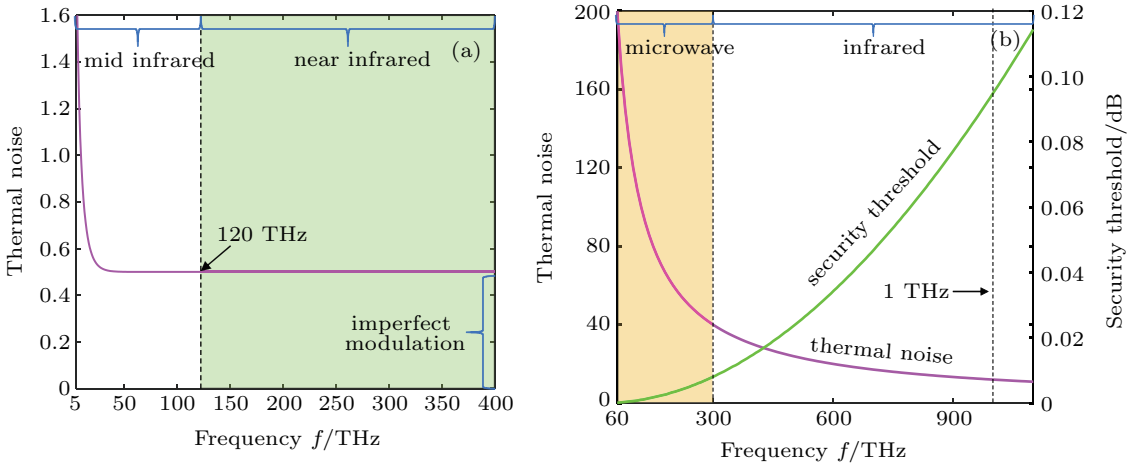


Fig. 3. (a) Near-and-mid infrared band and (b) terahertz band.

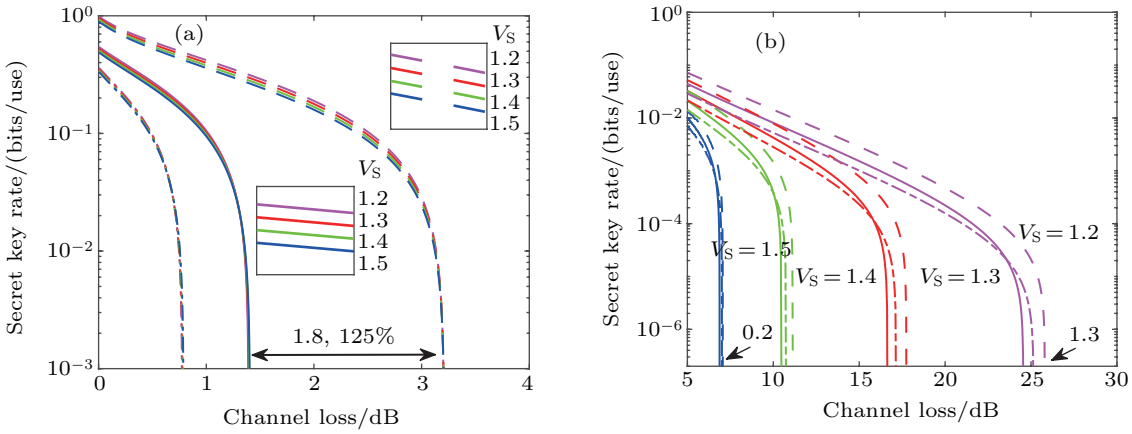


Fig. 4. Secret key rate as a function of channel loss (dB) using (a) Direct reconciliation (b) reverse reconciliation. The solid line is the standard TS-CVQKD, while the dashed line represents the HLA-involved TS-CVQKD with $g_{\mathrm{NLA}} = 1.2$, $g_{\mathrm{DLA}} = \sqrt{20}$ in DR and $g_{\mathrm{NLA}} = 1.5$, $g_{\mathrm{DLA}} = \sqrt{20}$ in RR. The dash-dotted line represents the LOCM-involved TS-CVQKD with $\tau = 0.9$ and $\lambda = 1.02$ in both the cases.

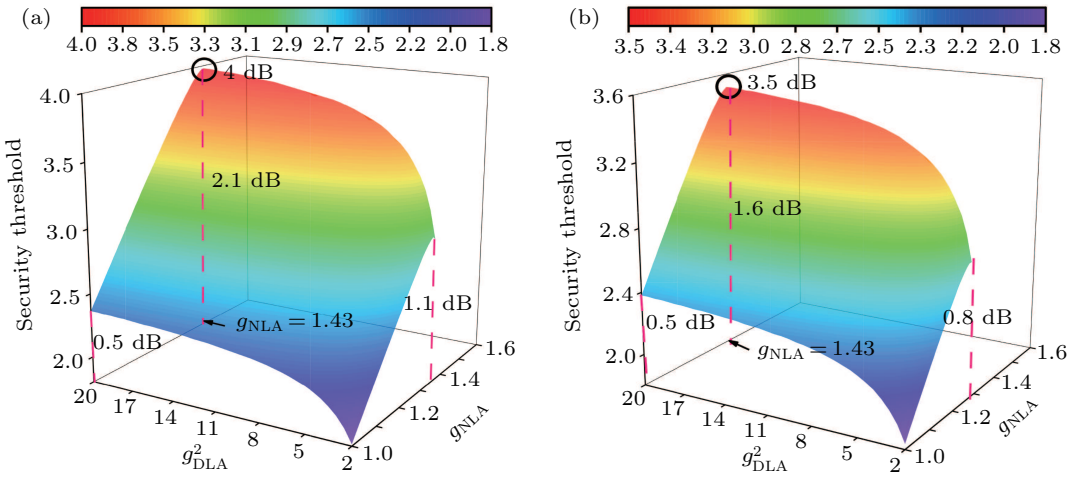


Fig. 5. Secure threshold of channel loss as functions of g_{DLA} and g_{NLA} in DR for (a) $f = 120$ THz and (b) $f = 6$ THz.

value of $g_{\rm NLA}$ will be shrunk from 1.43 to 1.34, and hence the improved security threshold declines to 1.6 dB. It is noteworthy that although the security threshold increases monotonically with both $g_{\rm NLA}$ and $g_{\rm DLA}$, the amplification effect of $g_{\rm NLA}$ on TS-CVQKD is more than that of $g_{\rm DLA}$ no matter what the frequency is, as shown by the dashed line in Fig. 5.

In Fig. 6, we find that the security threshold becomes the peak value (black circle) in RR for $g_{\rm DLA}=\sqrt{2}$ instead of $g_{\rm DLA}=\sqrt{20}$, which means that decreasing SNR of signal model can, at least within a certain range, improve security threshold. This situation is the so-called fighting noise with noise,[41] i.e., noise enhances the performance of TS-CVQKD. The same phenomenon can be seen for the parameter $g_{\rm NLA}$ as the peak value located at $g_{\rm NLA}=1.54$. At the same time, we also find HLA-involved TS-CVQKD in DR is superior to that in RR when the frequency drops quickly. In RR, the peak value fades from 7.52 dB to 0.8 dB as the frequency goes down from $f=120$ THz to $f=6$ THz. In DR, however, the peak value only slightly fades from 4 dB to 3.5 dB.

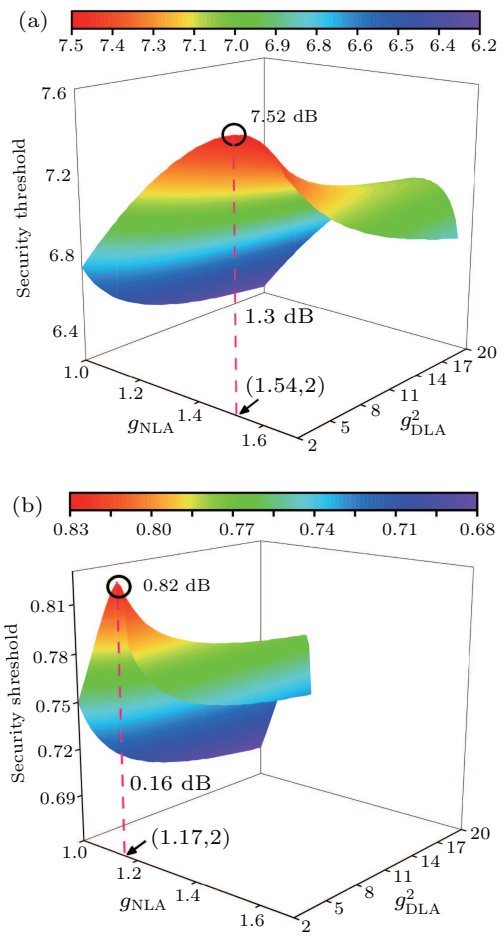


Fig. 6. Secure threshold of channel loss as functions of $g_{\rm DLA}$ and $g_{\rm NLA}$ in RR for (a) $f=120$ THz and (b) $f=6$ THz.

3.2. Terahertz band

It is known that thermal noise in terahertz band is extraordinary high. Even so, the terahertz band communication has some advantages for future wireless communication since the terahertz wave can integrate advantages of microwave and optical wave. Compared with the microwave communication, the terahertz communication possesses larger capacity and better direction. Compared with the optical wave, the terahertz wave holds advantages of high energy efficiency and good penetrability.[43] In addition, it allows to transfer huge messages very quickly and expects to offer applications for high speed data links.[44,45]

As shown in Fig. 3(b), the terahertz band is the bridge of microwave band and infrared band through boundary at 300 GHz. In near-and-mid infrared band, thermal noise is very tiny. However, it can be up to 200 in terahertz band at frequency of 60 GHz. Consequently, the security threshold is extremely small compared with that of near-and-mid infrared regime. Here we let $T_{\rm K}=15$ °C and $f\in\{1\ {\rm THz}, 300\ {\rm GHz}\}$ to demonstrate the amplification effect of the HLA-involved scheme. We focus on DR instead of RR since thermal noise here is extremely high and therefore DR is far beyond RR.

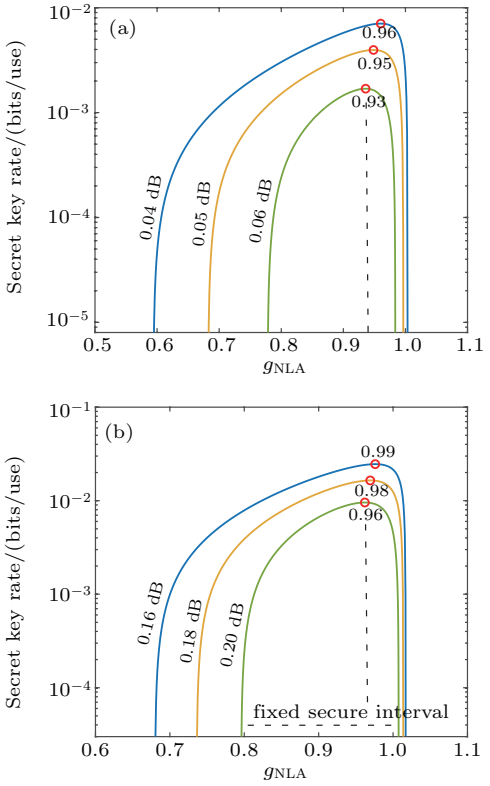


Fig. 7. The optical parameter $g_{\rm NLA}$ for the tunable channel loss at different frequencies: (a) channel loss fixed at $\{0.04, 0.05, 0.06\}$, (b) channel loss fixed at $\{0.16, 0.18, 0.20\}$.

Bob's electronic noise $v_{\rm el}$ will change when it comes to terahertz band. This electronic noise $v_{\rm el}$ is basically due to thermal noise introduced by the intrinsic amplifier circuit posterior to photon detection (not HLA) and it will still exist even when no signal light enters homodyne detector.[39] This thermal noise can be influenced by temperature, which means that one may use cryogenic amplifier circuit to suppress thermal fluctuations.[46] However, cryogenic amplifier circuit is too expensive for the practical implementation and hence we do not

apply this setup in the proposed scheme. As a result, the original noise should adopt to terahertz band and change to $v_{\rm el}N_0$.

In Fig. 7, we achieve the optimal value of $g_{\rm NLA}$ to maximize the secret key rate at $f = 300$ GHz and $f = 1$ THz. The parameter $g_{\rm NLA}$ must satisfy the restriction in Eq. (11). Thus, the $g_{\rm NLA}$ in terahertz band nearly cannot exceed 1 and thus the signal mode cannot be amplified. Fortunately, it has been pointed out that noiseless attenuation is also able to increase secret key rate and secure range of the protocol in the high-noise low-loss regime.[25] This inspires us because it happens to suit our case for high-noise and low-loss. Consequently, we consider the range of $g_{\rm NLA} < 1$ and obtain the optimal $g_{\rm NLA}$ for various channel loss. As shown in Fig. 7(b), the secret key rates reach the highest value for the optimized parameter $g_{\rm NLA} = 0.96$ in a fixed secure interval. As channel loss has been decreasing from 0.2 dB to 0.14 dB, the optimized parameter $g_{\rm NLA}$ will get closer to one and hence the fixed secure interval would become wider.

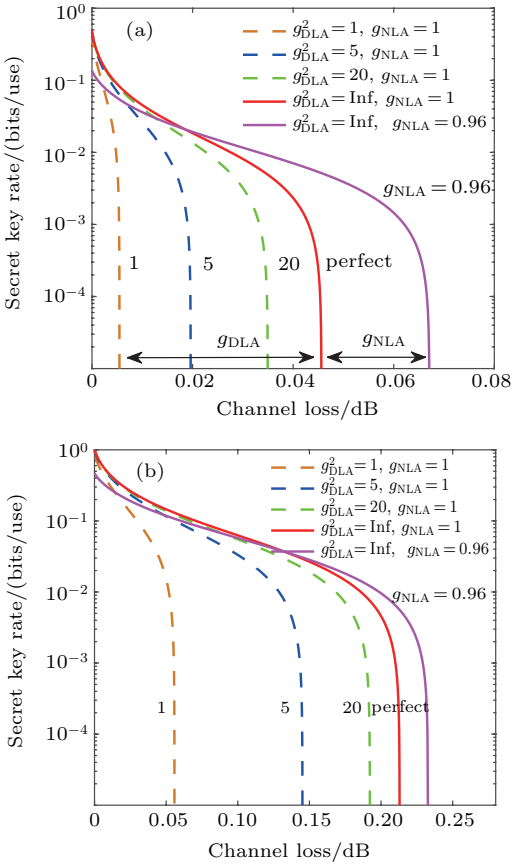


Fig. 8. The secret key rates versus channel loss in terahertz band with the tunable parameters $g_{\rm NLA}$ and $g_{\rm DLA}$ for (a) $f = 300$ GHz and (b) $f = 1$ THz. The three dashed lines show the secret key rates as $g_{\rm DLA}$ is increased from 1 to $\sqrt{20}$ without amplification effect of $g_{\rm NLA}$. The purple lines signify the secret key rates when $g_{\rm NLA} = 0.96$ is used on the basis of perfect detector.

As shown in Fig. 8, the performance of the HLA-involved TS-CVQKD can be improved in 300 GHZ and 1 THz. In Fig. 8, when $g_{\rm DLA}$ increases from 1 to $\sqrt{20}$, the imperfection of a practical detector will be compensated and $g_{\rm NLA}$ will further enhance the secret key rate. Although the HLA-involved scheme can still improve TS-CVQKD, which is similar to the counterpart in near-and-mid infrared band, there are different results. The parameter $g_{\rm DLA}$ plays a much more important role than $g_{\rm NLA}$. An ideal DLA can compensate for imperfections of Bob's practical detector in order to approach perfect detection apparatus. In near-and-mid infrared band, the electronic noise $v_{\rm el}$ is relative small so that $g_{\rm DLA}$ will not help too much. However, the electronic noise is much higher in terahertz band and therefore sensitive to $g_{\rm DLA}$.

In addition, controlling channel noise is another useful approach for enhancing the secret key rate. In the above analysis, we demonstrate that the HLA-involved scheme is relative robust against thermal noise in DR. However, we should point out that channel noise $V_{\rm E}$, unlike thermal noise, can dominate the HLA-involved scheme in the very limited range of security. The smaller the channel noise $V_{\rm E}$, the greater the secure distance. In Fig. 9, we compare the secret key rates with and without HLA for $V_{\rm E} \in \{5, 12, 20\}$. When $V_{\rm E}$ decreases from 20 (green dashed line) to 5 (red dashed line), the maximal transmission distance of the HLA-involved TS-CVQKD will be extended from 15 cm to 56 cm. We note that 56 cm, despite being a small secure region, is enough for some specific scenarios in near field communication (NFC, 10 cm), such as mobile payment and access control system.

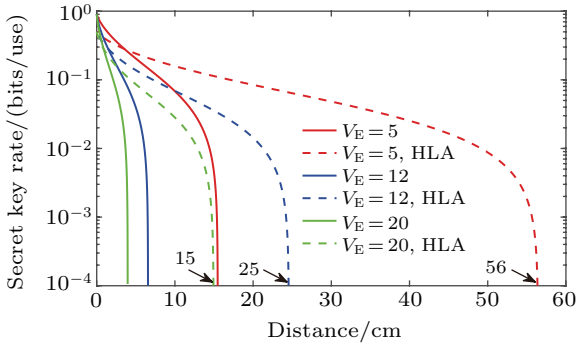


Fig. 9. How channel noise $V_{\rm E}$ influences the security of CVQKD with (dashed line, $g_{\rm DLA} = \sqrt{20}$, $g_{\rm NLA} = 0.96$) and without HLA (solid line) at $f = 1$ THz. The green, blue, and red line denote $V_{\rm E} = 5$, 12, 20 respectively. The attenuation is around 850 dB/km. A decrease in channel noise $V_{\rm E}$ will enhance the performance of TS-CVQKD protocol rapidly.

4. Conclusion

We have proposed an HLA-involved scheme for performance improvement of TS-CVQKD. Numerical simulations show that inserting an HLA before Bob's detector can enhance the security of TS-CVQKD no matter in near-and-mid infrared band or terahertz band. The direction of reconciliation and the frequency will influence performance of TS-CVQKD. We find that at 300 GHz and 1 THz, the optimal parameter $g_{\rm NLA}$ lies in the area of $g_{\rm NLA} < 1$, which is not only confined to 300 GHz and 1 THz but also suitable for all frequency band of high thermal radiation. In addition, the HLA-involved scheme can extend the maximal transmission distance at 1 THz from 15 cm to 56 cm, which indicates a potential application for not only NFC but also other wireless system requiring longer secure

distance. Furthermore, future work may extend this scheme deeply to microwave band (300 MHz–300 GHz) which seems more attractive in the microwave regime.[47,48]

Appendix A: Calculation of von Neumann entropy

In this Appendix, we will give the formulas about how to calculate von Neumann entropy of a 4×4 two-mode covariance matrix γ characterized as

$$\gamma=\begin{pmatrix}A & C\\ C & B\end{pmatrix}, \tag{A1}$$

where A, B, C are all 2×2 matrix.

Firstly, we need to find symplectic eigenvalues $v_{1,2}$ of γ

$$v_{1,2}^2=\frac{1}{2}[\Delta\pm\sqrt{\Delta^2-4\det\gamma}], \tag{A2}$$

where $\det\gamma$ is the determinant of the covariance matrix γ and $\Delta=\det A+\det B+2\det C$ are global symplectic invariants.

After finishing the calculation of symplectic eigenvalues, we need to plug $v_{1,2}$ into the following equation to obtain the von Neumann entropy S.

$$S=g(v_1)+g(v_2), \tag{A3}$$

where

$$g=\left(\frac{v+1}{2}\right)\log_2\left(\frac{v+1}{2}\right)-\left(\frac{v-1}{2}\right)\log_2\left(\frac{v-1}{2}\right). \tag{A4}$$

Appendix B: Calculation of secret key rate

In this Appendix, we will specify the calculative process to obtain the secret key rates for HLA-involved TS-CVQKD in both RR and DR respectively. For standard TS-CVQKD, we emphasize that it is only a particular case of $g_{\rm NLA}=g_{\rm DLA}=1$.

The secret key rates is given by

$$K=\beta I_{\rm AB}-(S(E)-S(E|b)), \tag{B1}$$

where $I_{\rm AB}$ is the mutual information between Alice and Bob, $S(E)$ and $S(E|b)$ describe the total and conditional von Neumann entropies of Eve's EPR states.

The first step is to calculate the mutual information $I_{\rm AB}$. As we can see from Fig. 1, the output variance of mode B_1, E_3 and E_1 is given by

$$V_{\rm B_1}=TV+(1-T)V_{\rm E}, \tag{B2}$$

$$V_{\rm E_3}=TV_{\rm E}+(1-T)V, \tag{B3}$$

$$V_{\rm E_1}=V_{\rm E}. \tag{B4}$$

After mode B_2 entered HLA, the action of NLA will change $V_{\rm B_2}$ via Eq. (6), which is described as

$$V_{\rm B_2}=\frac{V_{\rm B_1}+1+g_{\rm NLA}^2(V_{\rm B_1}-1)}{V_{\rm B_1}+1-g_{\rm NLA}^2(V_{\rm B_1}-1)}. \tag{B5}$$

Then, we use the joint action of DLA and imperfection of detector to obtain $V_{\rm B4}$,

$$\begin{aligned}V_{\rm B_4}&=\eta g_{\rm DLA}^2V_{\rm B_2}+(1-\eta)V_N=\eta g_{\rm DLA}^2\frac{V_{\rm B_1}+1+g_{\rm NLA}^2(V_{\rm B_1}-1)}{V_{\rm B_1}+1-g_{\rm NLA}^2(V_{\rm B_1}-1)}+(1-\eta)\left(1+\frac{v_{\rm el}}{1-\eta}\right)\\&=\eta g_{\rm DLA}^2\frac{TV+(1-T)V_{\rm E}+1+g_{\rm NLA}^2(TV+(1-T)V_{\rm E}-1)}{TV+(1-T)V_{\rm E}+1-g_{\rm NLA}^2(TV+(1-T)V_{\rm E}-1)}+1-\eta+v_{\rm el}.\end{aligned} \tag{B6}$$

In order to obtain the mutual information $I_{\rm AB}$, we still need to find conditional variance $V_{\rm B4|a}$. This is realized by replacing V with shot noise $V_{\rm S}$ in Eq. (B6),

$$V_{\rm B_4|a}=\eta g_{\rm DLA}^2\frac{TV_{\rm S}+(1-T)V_{\rm E}+1+g_{\rm NLA}^2(TV_{\rm S}+(1-T)V_{\rm E}-1)}{TV_{\rm S}+(1-T)V_{\rm E}+1-g_{\rm NLA}^2(TV_{\rm S}+(1-T)V_{\rm E}-1)}+1-\eta+v_{\rm el}. \tag{B7}$$

Using Eqs. (B6) and (B7) we can calculate Alice and Bob's mutual information $I_{\rm AB}$ to be

$$I_{\rm AB}=\frac{1}{2}\log_2\left(\frac{V_{\rm B_4}}{V_{\rm B_4|a}}\right). \tag{B8}$$

The second step is to obtain Eve's entropy $S(E)$. After interaction with signal mode, Eve's covariance matrix is made up from two modes E_1 and E_3,

$$\gamma_{\rm E_2E_3}=\begin{pmatrix}{\rm diag}[V_{\rm E_3},V_{\rm E_3}] & \varphi\boldsymbol{Z}\\ \varphi\boldsymbol{Z} & V_{\rm E_1}\boldsymbol{I}\end{pmatrix}, \tag{B9}$$

where $\varphi=[T(V_{\rm E_1}^2-1)]^2$ and the symbol "diag" represents a matrix with equal numerical value of diagonal elements and zeros anywhere else. $\boldsymbol{Z}$ and $\boldsymbol{I}$ are given by

$$\boldsymbol{Z}=\begin{pmatrix}1 & 0\\ 0 & -1\end{pmatrix},\quad \boldsymbol{I}=\begin{pmatrix}1 & 0\\ 0 & 1\end{pmatrix}. \tag{B10}$$

In the usual case, Eve's covariance matrix $\gamma_{\rm E_2E_3}$ will remain until Bob has conducted his measurement. However, due to the effect of NLA, Eve's CM $\gamma_{\rm E_2E_3}$ will make a difference and changes to

$$\gamma_{\rm E_2'E_3'}=\begin{pmatrix}{\rm diag}[V'_{\rm E_3},V'_{\rm E_3}] & c_{E_2'E_3'}\boldsymbol{Z}\\ c_{E_2'E_3'}\boldsymbol{Z} & {\rm diag}[V'_{\rm E_2},V'_{\rm E_2}]\end{pmatrix}, \tag{B11}$$

where

$$V'_{\mathrm{E}_3} = \frac{(1-T)V + TV_{\mathrm{E}} + VV_{\mathrm{E}} + g^2_{\mathrm{NLA}}(TV_{\mathrm{E}} - VV_{\mathrm{E}} + (1-T)V)}{V_{\mathrm{E}} + TV - TV_{\mathrm{E}} - V_{\mathrm{E}}g^2_{\mathrm{NLA}} + g^2_{\mathrm{NLA}} - TVg^2_{\mathrm{NLA}} + TV_{\mathrm{E}}g^2_{\mathrm{NLA}} + 1}, \tag{B12}$$

$$V'_{\mathrm{E}_2} = V_{\mathrm{E}} - \frac{(V^2_{\mathrm{E}} - 1)(g^2_{\mathrm{NLA}} - 1)(T-1)}{V_{\mathrm{E}} + TV - TV_{\mathrm{E}} - V_{\mathrm{E}}g^2_{\mathrm{NLA}} + g^2_{\mathrm{NLA}} - TVg^2_{\mathrm{NLA}} + TV_{\mathrm{E}}g^2_{\mathrm{NLA}} + 1}, \tag{B13}$$

$$c_{\mathrm{E}'_2\mathrm{E}'_3} = \frac{\sqrt{T(V^2_{\mathrm{E}} - 1)}(V - Vg^2_{\mathrm{NLA}} + g^2_{\mathrm{NLA}} + 1)}{V_{\mathrm{E}} + TV - TV_{\mathrm{E}} - V_{\mathrm{E}}g^2_{\mathrm{NLA}} + g^2_{\mathrm{NLA}} - TVg^2_{\mathrm{NLA}} + TV_{\mathrm{E}}g^2_{\mathrm{NLA}} + 1}. \tag{B14}$$

After we get CM of Eve, we can obtain the von Neumann entropies $S(E)$ by the method showed in Appendix A.

The third step is to obtain Eve's conditional entropy $S(E|b)$. After mode $B4$ has been measured using homodyne detection, $\gamma_{\mathrm{E}'_2\mathrm{E}'_3}$ can be converted as[11]

$$\gamma_{\mathrm{E}'_2\mathrm{E}'_3|\mathrm{b}} = \gamma_{\mathrm{E}'_2\mathrm{E}'_3} - (V^{-1}_{\mathrm{B}_4})\boldsymbol{X}\prod\boldsymbol{X}^T, \tag{B15}$$

where

$$\prod = \begin{pmatrix} 1 & 0 \\ 0 & 0 \end{pmatrix}, \tag{B16}$$

and $\boldsymbol{X}$ denote the correlations between EPR states E_2, E_4 and mode B_4. It is described as

$$\boldsymbol{X} = \begin{pmatrix} <\hat{E}'_2\hat{X}_{\mathrm{B}_4}>\boldsymbol{I} \\ <\hat{E}'_3\hat{X}_{\mathrm{B}_4}>\boldsymbol{I} \end{pmatrix} = \begin{pmatrix} <\sqrt{\eta g_{\mathrm{DLA}}}\hat{E}'_2\hat{X}_{\mathrm{B}_3}>\boldsymbol{I} \\ <\sqrt{\eta g_{\mathrm{DLA}}}\hat{E}'_3\hat{X}_{\mathrm{B}_3}>\boldsymbol{I} \end{pmatrix}, \tag{B17}$$

where $\langle\hat{E}'_2\hat{X}_{\mathrm{B}_3}\rangle$ and $\langle\hat{E}'_3\hat{X}_{\mathrm{B}3}\rangle$ can also be calculated using Eq. (6). It is given by

$$\langle\hat{E}'_2\hat{X}_{\mathrm{B}_3}\rangle = \frac{2g_{\mathrm{NLA}}\sqrt{(V^2_{\mathrm{E}} - 1)(1-T)}}{V_{\mathrm{E}} + TV - TV_{\mathrm{E}} - V_{\mathrm{E}}g^2_{\mathrm{NLA}} + g^2_{\mathrm{NLA}} - TVg^2_{\mathrm{NLA}} + TV_{\mathrm{E}}g^2_{\mathrm{NLA}} + 1}, \tag{B18}$$

$$\langle\hat{E}'_3\hat{X}_{\mathrm{B}_3}\rangle = \frac{-2g_{\mathrm{NLA}}(V - V_{\mathrm{E}}\sqrt{T(1-T)})}{V_{\mathrm{E}} + TV - TV_{\mathrm{E}} - V_{\mathrm{E}}g^2_{\mathrm{NLA}} + g^2_{\mathrm{NLA}} - TVg^2_{\mathrm{NLA}} + TV_{\mathrm{E}}g^2_{\mathrm{NLA}} + 1}. \tag{B19}$$

Now, we get the covariance matrix $\gamma_{\mathrm{E}'_2\mathrm{E}'_3}$ and $\gamma_{\mathrm{E}'_2\mathrm{E}'_3|\mathrm{b}}$ in Eqs. (B11) and (B15), respectively. Using these CM, the von Neumann entropies of $S(E)$ and $S(E|b)$ can be computed as shown in Appendix A but are not written down explicitly here due to their lengths. Finally, we can get the secret key rates as three components of $K(I_{\mathrm{AB}}, \gamma_{\mathrm{E}'_2\mathrm{E}'_3}, \gamma_{\mathrm{E}'_2\mathrm{E}'_3|\mathrm{b}})$ are all determined.

The secret key rates for DR using homodyne detection is given by

$$K = \beta I_{\mathrm{AB}} - (S(E) - S(E|a)). \tag{B20}$$

Here the calculation would be much more simple since I_{AB} and $\gamma_{\mathrm{E}'_2\mathrm{E}'_3}$ have already been shown in Eqs. (B8) and (B11). The only thing we need to do is to calculate covariance matrix $\gamma_{\mathrm{E}'_2\mathrm{E}'_3|\mathrm{a}}$, which can be obtained by replacing V'_{E_2}, V'_{E_3}, and $c_{\mathrm{E}'_2\mathrm{E}'_3}$ in by

$$V'_{\mathrm{E}_3|\mathrm{a}} = \frac{(1-T)V_{\mathrm{S}} + TV_{\mathrm{E}} + V_{\mathrm{S}}V_{\mathrm{E}} + g^2_{\mathrm{NLA}}(TV_{\mathrm{E}} - V_{\mathrm{S}}V_{\mathrm{E}} + (1-T)V_{\mathrm{S}})}{V_{\mathrm{E}} + TV_{\mathrm{S}} - TV_{\mathrm{E}} - V_{\mathrm{E}}g^2_{\mathrm{NLA}} + g^2_{\mathrm{NLA}} - TV_{\mathrm{S}}g^2_{\mathrm{NLA}} + TV_{\mathrm{E}}g^2_{\mathrm{NLA}} + 1}, \tag{B21}$$

$$V'_{\mathrm{E}_2|\mathrm{a}} = V_{\mathrm{E}} - \frac{(V^2_{\mathrm{E}} - 1)(g^2_{\mathrm{NLA}} - 1)(T-1)}{V_{\mathrm{E}} + TV_{\mathrm{S}} - TV_{\mathrm{E}} - V_{\mathrm{E}}g^2_{\mathrm{NLA}} + g^2_{\mathrm{NLA}} - TV_{\mathrm{S}}g^2_{\mathrm{NLA}} + TV_{\mathrm{E}}g^2_{\mathrm{NLA}} + 1}, \tag{B22}$$

$$c_{\mathrm{E}'_2\mathrm{E}'_3|\mathrm{a}} = \frac{\sqrt{T(V^2_{\mathrm{E}} - 1)}(V_{\mathrm{S}} - V_{\mathrm{S}}g^2_{\mathrm{NLA}} + g^2_{\mathrm{NLA}} + 1)}{V_{\mathrm{E}} + TV_{\mathrm{S}} - TV_{\mathrm{E}} - V_{\mathrm{E}}g^2_{\mathrm{NLA}} + g^2_{\mathrm{NLA}} - TV_{\mathrm{S}}g^2_{\mathrm{NLA}} + TV_{\mathrm{E}}g^2_{\mathrm{NLA}} + 1}. \tag{B23}$$

This is realized by changing $V \to V_{\mathrm{S}}$ in Eq. (B11).[16] We emphasize that this replacement is only conducted in anyone of quadrature $\hat{Q}$ ($\hat{P}$) and the other quadrature $\hat{P}$ ($\hat{Q}$) would remain unchanged as denoted in Eq. (B11), because we use homodyne detection here instead of heterdyne detection.

Y. H. accomplished the formula derivation and numerical simulations and drafted the article. Y. G. provided feasible advice and critical revision of the manuscript. H. Z. provided critical advice and reviewed relevant studies and literature. D. H. performed critical revision of the manuscript. All authors have read and approved the final manuscript.

References

[1] Scarani V, Bechmann-Pasquinucci H, Cerf N J, Dušek M, Lütkenhaus N and Peev M 2009 *Rev. Mod. Phys.* **81** 1301

[2] Grosshans F, Van Assche G, Wenger J, Brouri R, Cerf N J and Grangier P 2003 *Nature* **421** 238

[3] Zhang S J, Ma H X, Wang X, Zhou C, Bao W S and Zhang H L 2019 *Chin. Phys. B* **28** 080304

[4] Gong L H, Song H C, He C S, Liu Y and Zhou N R 2014 *Phys. Scr.* **89** 035101

[5] Gessner M, Pezze L and Smerzi A 2016 *Phys. Rev. A* **94** 020101

[6] Takeda S, Fuwa M, van Loock P and Furusawa A 2015 *Phys. Rev. Lett.* **114** 100501

[7] Yin J, Cao Y, Li Y H *et al.* 2017 *Science* **356** 1140

[8] Du G H, Li H W, Wang Y and Bao W S 2019 *Chin. Phys. B* **28** 90301

[9] He R S, Jiang M S, Wang Y, Gan Y H, Zhou C and Bao W S 2019 *Chin. Phys. B* **28** 040303

[10] Zhang Y, Li Z, Chen Z *et al.* 2019 *Quantum Sci. Technol.* **4** 035006

[11] Weedbrook C, Pirandola S, García-Patrón R, Cerf N J, Ralph T C, Shapiro J H and Lloyd S 2012 *Rev. Mod. Phys.* **84** 621

[12] Qi B, Huang L L, Qian L and Lo H K 2007 *Phys. Rev. A* **76** 052323

[13] Fossier S, Diamanti E, Debuisschert T, Villing A, Tualle-Brouri R and Grangier P 2009 *New J. Phys.* **11** 045023

[14] Liao Q, Wang Y, Huang D and Guo Y 2018 *Opt. Express* **26** 19907

[15] Newton E, Ghesquière A, Wilson F L, Varcoe B T and Moseley M 2019 *J. Phys. B-At. Mol. Opt. Phys.* **52** 125501

[16] Weedbrook C, Pirandola S and Ralph T C 2012 *Phys. Rev. A* **86** 022318

[17] Weedbrook C, Ottaviani C and Pirandola S 2014 *Phys. Rev. A* **89** 012309

[18] Papanastasiou P, Ottaviani C and Pirandola S 2018 *Phys. Rev. A* **98** 032314

[19] Lu Z, Shi J H and Li F G 2017 *Chin. Phys. B* **26** 040304

[20] Qi B, Evans P G and Grice W P 2018 *Phys. Rev. A* **97** 012317

[21] Wu X, Wang Y, Li S, Zhang W, Huang D and Guo Y 2019 *Quantum Inf. Process* **18** 372

[22] Usenko V C and Filip R 2010 *Phys. Rev. A* **81** 022318

[23] Jacobsen C S, Gehring T and Andersen U L 2015 *Entropy* **17** 4654

[24] Blandino R, Leverrier A, Barbieri M, Etesse J, Grangier P and Tualle-Brouri R 2012 *Phys. Rev. A* **86** 012327

[25] Fiurášek J and Cerf N J 2012 *Phys. Rev. A* **86** 060302

[26] Fossier S, Diamanti E, Debuisschert T, Tualle-Brouri R and Grangier P 2009 *J. Phys. B-At. Mol. Opt. Phys.* **42** 114014

[27] Haw J Y, Zhao J, Dias J, Assad S M, Bradshaw M, Blandino R, Symul T, Ralph T C and Lam P K 2016 *Nat. Commun.* **7** 13222

[28] Yang F and Qiu D 2020 *Quantum Inf. Process* **19** 99

[29] Wang T, Yu S, Zhang Y C, Gu W and Guo H 2014 *Phys. Lett. A* **378** 2808

[30] Chen L Q, Sheng Y B and Zhou L 2019 *Chin. Phys. B* **28** 010302

[31] Walk N, Lund A P and Ralph T C 2013 *New J. Phys.* **15** 073014

[32] Ye W, Zhong H, Liao Q, Huang D, Hu L and Guo Y 2019 *Opt. Express* **27** 17186

[33] Osorio C I, Bruno N, Sangouard N, Zbinden H, Gisin N and Thew R T 2012 *Phys. Rev. A* **86** 023815

[34] Zhao J, Dias J, Haw J Y, Symul T, Bradshaw M, Blandino R, Ralph T, Assad S M and Lam P K 2017 *Optica* **4** 1421

[35] Zhou J, Shi R, Feng Y, Shi J and Guo Y 2019 *J. Phys. A-Math. Theor.* **52** 245303

[36] Pirandola S, Braunstein S L and Lloyd S 2008 *Phys. Rev. Lett.* **101** 200504

[37] Guo Y, Ye W, Zhong H and Liao Q 2019 *Phys. Rev. A* **99** 032327

[38] Zhang S J, Xiao C, Zhou C, Wang X, Yao J S, Zhang H L and Bao W S 2020 *Chin. Phys. B* **29** 20301

[39] Jouguet P, Kunz-Jacques S, Diamanti E and Leverrier A 2012 *Phys. Rev. A* **86** 032309

[40] Chrzanowski H M, Walk N, Assad S M, Janousek J, Hosseini S, Ralph T C, Symul T and Lam P K 2014 *Nat. Photon.* **8** 333

[41] Wang M J and Pan W 2010 *Phys. Lett. A* **374** 2434

[42] Milicevic M, Feng C, Zhang L M and Gulak P G 2017 *EPJ. Quantum Technol.* **4** 1

[43] Liu X, Zhu C, Chen N and Pei C 2018 *Quantum Inf. Process* **17** 304

[44] Sheikh F, Zarifeh N and Kaiser T 2016 *IET Microw. Antennas Propag.* **10** 1435

[45] Han C, Bicen A O and Akyildiz I F 2014 *IEEE Trans. Wirel. Commun.* **14** 2402

[46] Eom B H, Day P K, LeDuc H G and Zmuidzinas J 2012 *Nat. Phys.* **8** 623

[47] Pogorzalek S, Fedorov K G, Xu M *et al.* 2019 *Nat. Commun.* **10** 1

[48] Di Candia R, Fedorov K G, Zhong L, Felicetti S, Menzel E P, Sanz M, Deppe F, Marx A, Gross R and Solano E 2015 *EPJ. Quantum Technol.* **2** 25